Title

Mechanical Detection and Imaging of Hyperbolic Phonon Polaritons in Hexagonal Boron Nitride

Journal

ACS Nano, 11(9)

ISSN

1936-0851

Authors

Ambrosio, Antonio
Jauregui, Luis A
Dai, Siyuan
et al.

Publication Date

2017-09-26

DOI

10.1021/acsnano.7b02323

Peer reviewed

ACS NANO

www.acsnano.org

ARTICLE

Mechanical Detection and Imaging of Hyperbolic Phonon Polaritons in Hexagonal Boron Nitride

Antonio Ambrosio,[*,†,‡,§] Luis A. Jauregui,[‡] Siyuan Dai,[∥] Kundan Chaudhary,[⊥] Michele Tamagnone,[⊥] Michael M. Fogler,[∥] Dimitri N. Basov,[∥,#] Federico Capasso,[⊥] Philip Kim,[‡] and William L. Wilson[†]

[†]Center for Nanoscale Systems, [‡]Department of Physics, and [⊥]Harvard John A. Paulson School of Engineering and Applied Sciences, Harvard University, Cambridge, Massachusetts 02138, United States

[§]CNR-SPIN U.O.S. Napoli, Complesso Universitario di Monte Sant'Angelo, Via Cintia, 80126 Napoli, Italy

[∥]Department of Physics, University of California, San Diego, La Jolla, California 92093, United States

[#]Department of Physics, Columbia University, 538 West 120th Street, New York, New York 10027, United States

Supporting Information

ABSTRACT: **Mid-infrared nanoimaging and spectroscopy of two-dimensional (2D) materials have been limited so far to scattering-type scanning near-field optical microscopy (s-SNOM) experiments, where light from the sample is scattered by a metallic-coated atomic force microscope (AFM) tip interacting with the material at the nanoscale. These experiments have recently allowed imaging of plasmon polaritons in graphene as well as hyperbolic phonon polaritons in hexagonal boron nitride (hBN). Here we show that the high mechanical sensitivity of an AFM cantilever can be exploited for imaging hyperbolic phonon polaritons in hBN. In our imaging process, the lattice vibrations of hBN micrometer-sized flakes are locally enhanced by the launched phonon polaritons. These enhanced vibrations are coupled to the AFM tip in contact with the sample surface and recorded during scanning. Imaging resolution of Δ/20 is shown (Δ being the polaritonic fringes' separation distance), comparable to the best resolution in s-SNOM. Importantly, this detection mechanism is free from light background, and it is in fact the first photonless detection of phonon polaritons.**

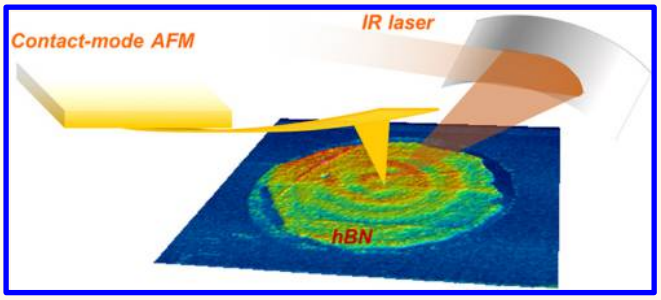

KEYWORDS: *hexagonal boron nitride, photothermal microscopy, phonon polaritons, nanoimaging, atomic force microscopy, scanning near-field optical microscopy*

The first atomic force microscope (AFM) was evocatively labeled "touching microscope" to convey that the microscope "feels" the sample's atoms and can produce an atomically resolved image of the surface. In their first paper "Atomic Force Microscope",[1] Binning, Quate, and Gerber had already envisioned a general-purpose device "that will measure any type of force; not only interatomic forces, but electromagnetic forces as well". Today, the AFM is really a general-purpose device used in many configurations for specific force characterization, including electric force microscopy,[2,3] magnetic force microscopy,[4,5] microwave impedance microscopy,[6,7] multifrequency force microscopy,[8] *etc.* In its most recent applications AFM has also been proposed in different schemes for optical near-field imaging[9−13] and spectroscopy at the nanoscale without detecting any light.[14−19]

In this paper, we show imaging of optically excited hyperbolic phonon polaritons (HP^2) in hexagonal boron nitride (hBN) flakes by monitoring only the mechanical oscillations induced in an AFM cantilever.

Phonon polaritons, as well as surface plasmon polaritons (SPPs), have attracted great interest for many years due to their role as energy carriers.[20−22] In fact, directional control of electromagnetic energy propagation in flat optoelectronic devices needs strong coupling of electromagnetic waves to local material excitations. SPPs are generated by collective excitations of electrons (*e.g.*, at a metal−dielectric interface), while an electromagnetic wave coupled to the lattice vibrations (phonons) of a polar crystal gives rise to the excitation of phonon polaritons.

Received: April 3, 2017
Accepted: August 31, 2017
Published: August 31, 2017

DOI: 10.1021/acsnano.7b02323
ACS Nano 2017, 11, 8741−8746

Hexagonal boron nitride is of particular interest in terms of phonon polaritons since it has been found to have low-loss phonon polaritons in the upper Reststrahlen band (1370−1610 cm^{-1}). Moreover, in this wavelength (wavenumbers) range (type II band), hBN is hyperbolic, *i.e.* $\varepsilon_z > 0$ and $\varepsilon_t < 0$, where ε_z and ε_t are the axial (normal to the surface) and tangential (in plane) permittivities, respectively.[23−29] In fact, due to the momentum mismatch between the free space illuminating light and the highly confined propagating polaritons, a local scatterer (point of origin) close to the sample surface is needed to launch phonon polariton propagating waves.[30]

Hyperbolic phonon polaritons have been previously imaged in hBN by means of scattering-type scanning near-field optical microscopy (s-SNOM).[31,32] In this configuration, as reported in ref 31, an hBN flake is usually shaped in a triangle by electron beam lithography and reactive ion etching (Supporting Information). The local scatterer that allows overcoming the momentum mismatch is the metal-coated tip of the s-SNOM microscope illuminated by mid-IR light at an angle.[33−35] The presence of sharp edges like in hBN flakes with a well-defined geometric shape of several micrometers is important since hyperbolic phonon polaritons have low losses, and, by reflecting at the edges, they create standing waves that are then visualized during the imaging process.[36−39] Described more explicitly, (1) the tip launches the phonon polariton; (2) the polariton propagates and is reflected at the edges of the flake, creating a standing wave that may have a minimum, a maximum, or any intermediate amplitude at the tip position; and (3) the tip scatters the radiation to open air for far-field detection by means of a mid-IR detector. Figure 1a and b show the amplitude and phase of the near-field scattered light (s-SNOM signal) from the surface of a 67 nm thick hBN flake on 285 nm thick SiO_2. The phonon polariton standing wave is clearly visible. The s-SNOM microscope used here is the same as that in ref 31 (Neaspec GmbH).

RESULTS AND DISCUSSION

The detection scheme presented here is still based on an atomic force microscopy platform, but no radiation is detected. Imaging of the HP^2 is obtained by monitoring only the mechanical oscillations of the microscope cantilever (Figure 1c). This detection is then free from light background. The detection scheme is similar to both photothermal microscopy and photoinduced force microscopy, where a light-driven local surface−tip interaction (local heating or optical forces) is monitored as induced mechanical oscillations on an AFM cantilever.[17] Also, while this paper was under review, we were informed of a recent work achieving chemical imaging by combining mid-IR illumination with peak force microscopy.[40]

In our microscope (Anasys Instruments) an infrared laser beam from an optical parametric oscillator (OPO) is focused onto the tip−sample region by means of a low numerical aperture parabolic mirror (Figure 1c). The laser is pulsed (10 ns pulse width, 1 kHz fixed repetition rate) and can be wavelength tuned in the upper Reststrahlen band of hBN (1370−1610 cm^{-1}). The microscope operates as an AFM in contact mode. That is, the tip (gold coated; nominal spring constant in the range 0.07−0.4 N/m; nominal resonance frequency of 13 kHz) is then not oscillated by an external dithering piezo; rather it is in "contact" with the sample surface. When the sample is illuminated, some oscillations on the microscope cantilever appear at around 170 kHz (one of the mechanical modes of the cantilever). Similarly to multi-frequency force microscopy,[8] operating on a secondary mechanical mode of the cantilever increases the quality factor of the cantilever and helps to improve the signal-to-noise ratio of the detected signal. Figure 1d shows the image ("photothermal" signal) that we obtained for the polariton standing

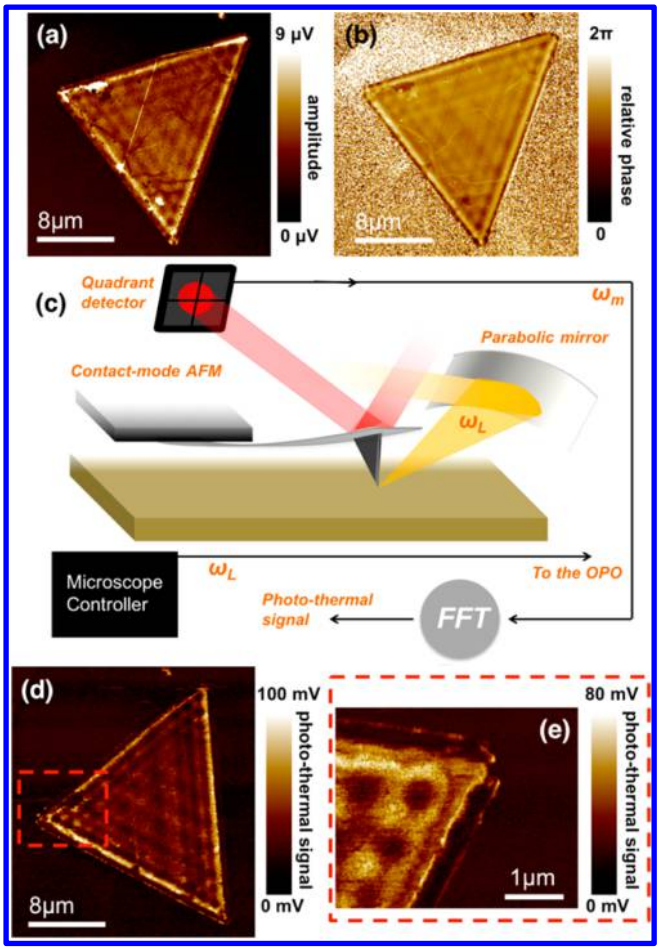

Figure 1. (a) Amplitude (in volts from the detector) and (b) phase (relative phase with respect to a gold-coated surface used as reference) of hyperbolic phonon polaritons imaged using s-SNOM. The hBN flake was shaped in a triangle of dimensions 16 μm × 16 μm × 18 μm using electron beam lithography and is on 285 nm thick SiO_2. The flake thickness is 67 nm, measured with atomic force microscopy in contact mode. (c) Schematic of the experimental setup for photothermal microscopy. A pulsed laser with repetition rate ω_L = 1 kHz (a mid-IR OPO laser) is focused to the tip−sample region by means of a parabolic mirror. In this imaging process, the microscope is operated with a gold-coated tip in contact with the sample surface. The tip launches the phonon polariton; the polariton propagates and is reflected at the edges of the flake, creating a standing wave; the light-induced oscillations at the sample surface are transferred to the tip that starts oscillating on its mechanical modes. Fourier transform of the tip oscillations, monitored through the quadrant detector, is performed to analyze the spectral content. The oscillation amplitude (in volts from the quadrant photodetector) at a specific frequency ω_m is then chosen (with a bandwidth of about 50 kHz) to be monitored and recorded. This frequency is usually around 170 kHz for the AFM cantilever we used. The recorded oscillation amplitude at ω_m is the "photothermal" signal used to generate figures (d) and (e). (d) Photothermal image of the hyperbolic phonon polariton pattern at the surface of the same flake of (a) and (b). (e) Zoomed-in photothermal image of one of the corners of the flake. The illuminating light has a wavenumber of 1440 cm^{-1}.

DOI: 10.1021/acsnano.7b02323
ACS Nano 2017, 11, 8741−8746

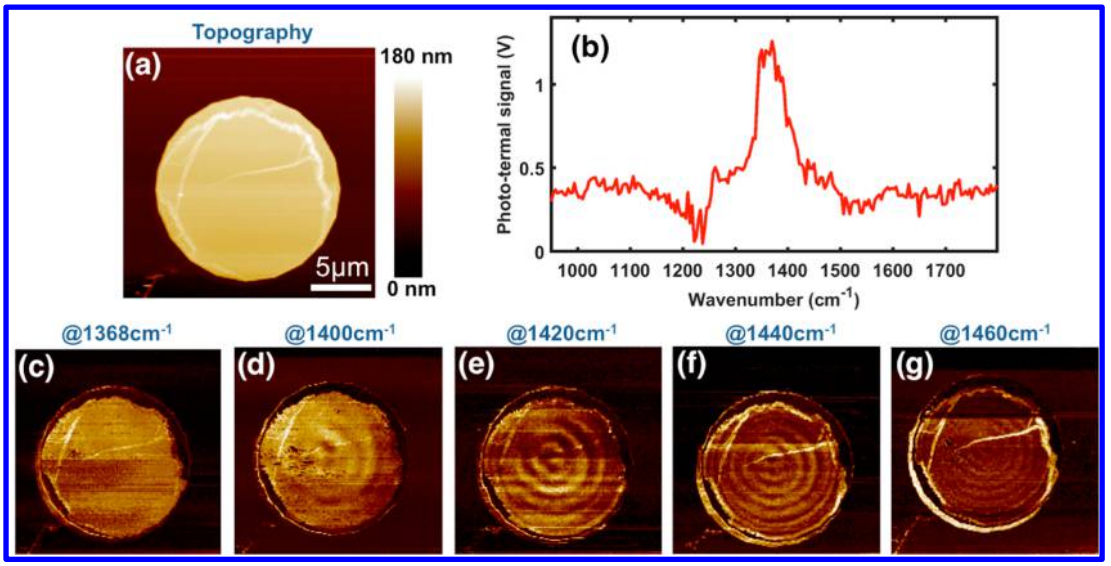

Figure 2. (a) Topography image of an hBN flake cut in the shape of a disk. The flake is on a Si substrate and is 140 nm thick. The flake diameter is 15 μm. (b) Photothermal signal as a function of the laser wavenumber. The position of the AFM tip in this case is in the central part of the flake. Signal is present in the type II band (1370−1610 cm^{-1}) with a peak around 1368 cm^{-1}. (c−g) Photothermal image of the hyperbolic phonon polariton pattern at different wavelengths (wavenumbers) of the illuminating light. The periodicity of the pattern decreases by increasing the wavenumber. Note that the patterns are concentric to the edges of the flake.

wave in the hBN flake. This image is then not obtained by detecting scattered light but by monitoring the amplitude of the induced oscillations on the cantilever at 170 kHZ (with a bandwidth of 50 kHz and a typical scanning rate of 0.1 Hz). There is complete superposition between the s-SNOM patterns shown in Figure 1a and b and that in Figure 1d (see also Figure S1). Figure 1e shows instead a zoomed-in image of the polariton pattern in a corner of the shaped flake. This figure clearly shows the possibility to visualize features only a couple of hundred nanometers wide (resolution of $\Delta/20$, Δ being the fringes' spacing), comparable to the best resolution achieved in mid-IR s-SNOM.

In our imaging process, the lattice vibrations are locally enhanced by the launched phonon polariton, spatially modulated by the polariton wave. These enhanced vibrations (on a macroscopic scale this corresponds to local heating and thermal expansion) are what in fact cause the induced tip oscillations (photothermal signal). More precisely, the repetition rate of the illuminating laser is 1 kHz. This results in periodic oscillations of the sample surface upon heating that are transferred to the microscope probe cantilever. The induced oscillations couple to several modes of the cantilever, including the mode around 170 kHz, whose amplitude is monitored during the imaging process. The surface oscillations at 1 kHz are slow with respect to the detection frequency of 170 kHz but fast enough to be not fully compensated by the microscope feedback; they turn then into induced oscillations of the cantilever that is in contact (AFM contact mode) with the sample surface.

Note that other phenomena can in principle contribute to the induced mechanical oscillations of the probe cantilever.

An enhanced radiative heat transfer, mediated by phonon polaritons, between two objects has been studied, for instance.[41,42] However, those experiments need to be carried under vacuum to get reasonable signal-to-noise ratio in the detection. We operated in air. Moreover, the largest enhancement of those experiments has been reported between similar polar crystals that support phonon polaritons at the same wavelength (near-field interaction of the polaritonic field). In our experiment instead, one of the objects, the microscope cantilever, is gold coated. For these reasons, it looks unrealistic that radiative heat transfer is our main sensing mechanism.

Direct forces of optical origin are also possible in principle. According to this picture, the evanescent tail of the phonon polariton in air would couple to the metallic tip, generating a weak optical force depending on the polariton local strength. This would be similar to the working principle of the photoinduced force microscopy technique.[43] However, in our experiment local heating of the sample surface is evident when the laser power approaches 1 mW (Supporting Information). For this, we also exclude optical forces at the sample surface as the main detection mechanism in our experiment.

In a complementary experiment we used an hBN flake, 140 nm thick, deposited on a Si substrate and cut in the shape of a disk (Figure 2). In this case we changed the wavelength of the illuminating light, observing how the polariton pattern periodicity changes (polariton dispersion): smaller wavenumbers result in lager fringe spacing (Figure S2). As shown in Figure 2b, when the microscope probe is on top of the hBN flake, the amplitude of the photothermal signal as a function of the laser wavenumber reflects the type II band with a maximum around 1368 cm^{-1}.[31] However, if the tip is right at the position where one of the bright fringes of the HP^2 standing wave is located for a specific wavelength, the photothermal signal recorded as a function of the illuminating wavenumber (photothermal spectrum) may show peaks at wavenumbers that produce the specific fringe. This case is illustrated in Figure 3c, where the photothermal spectrum shows a peak at 1440 cm^{-1}. In this case the microscope tip is positioned on top of one of the bright fringes produced on the surface when illuminating at 1440 cm^{-1} (Figure 3b red circle). A similar effect is also found in scattering near-field experiments (Figure S7).

All our samples of hBN flakes are on 285 nm SiO_2 (except that of Figure 2, which is on Si), which has a phonon resonance around 1100 cm^{-1}. Our imaging process is able to detect this

DOI: 10.1021/acsnano.7b02323
ACS Nano 2017, 11, 8741−8746

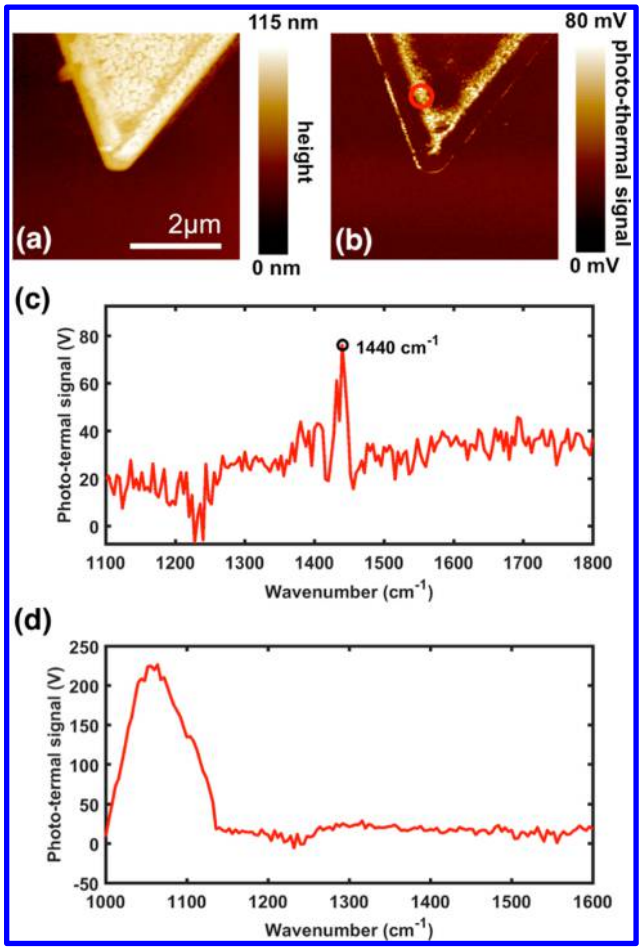

Figure 3. (a) Topography and (b) photothermal image at 1440 cm^{-1} of a corner of a triangle-shaped hBN flake. (c) Spectrum at the tip position highlighted by the red circle in (b). This spectrum is obtained by recording the photothermal signal while swiping the wavenumbers of the illuminating light for a fixed position of the tip. A peak at 1440 cm^{-1} is evident. This only happens when the tip is on top of a maximum of interference of the polariton beam. (d) Photothermal spectrum recorded when the tip is on the SiO_2 substrate. The phonon resonance of SiO_2 is clearly visible around 1100 cm^{-1}.

resonance as well. Figure 3d shows the photothermal spectrum when the microscope tip is on the SiO_2 substrate. High signal around the SiO_2 phonon peak is evident.

CONCLUSIONS

In this work we show that the interference patterns created by phonon polaritons in shaped flakes of hexagonal boron nitride can be imaged with high resolution by monitoring the mechanical oscillations of an AFM cantilever in contact with the sample surface. We show that this imaging process is based on local sample heating mediated by the phonon polariton resonances of hBN, although *ad hoc* experiments should be planned to better quantify contributions from other effects such as optical forces or the specific tip material.

This scheme is similar to photothermal microscopy that has shown the best results so far mainly on soft and easily deformable materials such as polymers.[44] Our imaging process provides the same features obtained in scattering near-field optical microscopy but does not require detecting any light and, as such, is a light-background-free photonless detection of the coupling of light to the crystal lattice oscillations. This result extends mid-IR nanoimaging and spectroscopy *via* mechanical detection based on an AFM probe to crystals, 2D materials, and van der Waals heterostructures.

MATERIALS AND METHODS

Sample Fabrication. Hexagonal boron nitride is mechanically exfoliated onto a 285 nm SiO_2/silicon or a bare silicon substrate with predefined metallic alignment marks. The substrates are then covered with MA-N 2403 (negative e-beam resist) and exposed to an e-beam system with a dose of 1200 $\mu C/cm^2$ using an accelerating voltage of 125 kV. The samples are shaped into triangles, circles, or rectangles. After developing in AZ-726 for 1 min, the samples are prebaked at 100 °C for 10 min. Then hBN is etched by using a reactive ion etching system with $CHF_3/Ar/O_2$ at flows of 10/5/2 sccm, respectively, and an RF generator at 30 W for 2−5 min.[45] After the etching process, exposed MA-N 2403 resist is removed by Remover PG and chloroform; afterward, the samples are rinsed with isopropyl alcohol and dried with nitrogen.

ASSOCIATED CONTENT

Supporting Information

The Supporting Information is available free of charge on the ACS Publications website at DOI: 10.1021/acsnano.7b02323.

Comparison between s-SNOM and photothermal imaging of phonon polaritons in hBN, periodicity trend of phonon polarion fringes in hBN on a Si substrate, description of the apparent change of sample height as an artifact of AFM imaging, comparison of samples before and after thermal annealing, nano-FTIR s-SNOM spectra on an hBN sample (PDF)

AUTHOR INFORMATION

Corresponding Author

*E-mail: ambrosio@seas.harvard.edu.

ORCID

Antonio Ambrosio: 0000-0002-8519-3862

Siyuan Dai: 0000-0001-7259-7182

Notes

The authors declare no competing financial interest.

ACKNOWLEDGMENTS

This work was performed in part at the Center for Nanoscale Systems (CNS), a member of the National Nanotechnology Coordinated Infrastructure (NNCI), which is supported by the National Science Foundation under NSF award no. 1541959. CNS is a part of Harvard University. S.N.D., M.F., and D.N.B. are supported by ONR N00014-15-1-2671. D.N.B. is the Moore Investigator in Quantum Materials EPIQS program GBMF4533. This work was supported by the National Science Foundation EFRI 2-DARE program through grant no. 1542807. M.T. acknowledges the support of the Swiss National Science Foundation (SNSF) grant no. 168545.

REFERENCES

(1) Benning, G.; Quate, C. F.; Gerber, Ch. Atomic Force Microscope. *Phys. Rev. Lett.* **1986**, *56*, 930−933.

(2) Bohm, C. Electric Force Microscopy: Gigahertz and Nanometer Measurement Tool. *Microelectron. Eng.* **1996**, *31*, 171−179.

(3) Yokoyama, H.; Inoue, T.; Itoh, J. Nonresonant Detection of Electric Force Gradients by Dynamic Force Microscopy. *Appl. Phys. Lett.* **1994**, *65*, 3143−3145.

DOI: 10.1021/acsnano.7b02323
ACS Nano 2017, 11, 8741−8746

(4) Hartmann, U. Magnetic Force Microscopy. *Adv. Mater.* **1990**, *2*, 550−552.
(5) Hartmann, U. Magnetic Force Microscopy: Some Remarks From the Micromagnetic Point of View. *J. Appl. Phys.* **1988**, *64*, 1561−1564.
(6) Seabron, E.; MacLaren, S.; Xie, X.; Rotkin, S. V.; Rogers, J. A.; Wilson, W. L. Scanning Probe Microwave Reflectivity of Aligned Single-Walled Carbon Nanotubes: Imaging of Electronic Structure and Quantum Behavior at the Nanoscale. *ACS Nano* **2016**, *10*, 360−368.
(7) Kundhikanjana, W.; Yang, Y.; Tanga, Q.; Zhang, K.; Lai, K.; Ma, Y.; Kelly, M. A.; Li, X. X.; Shen, Z. X. Unexpected Surface Implanted Layer in Static Random Access Memory Devices Observed by Microwave Impedance Microscope. *Semicond. Sci. Technol.* **2013**, *28*, 025010.
(8) Garcia, R.; Herruzo, E. The Emergence of Multifrequency Force Microscopy. *Nat. Nanotechnol.* **2012**, *7*, 217−226.
(9) Ambrosio, A.; Allegrini, M.; Latini, G.; Cacialli, F. Thermal Processes in Metal- Coated Fiber Probes for Near-Field Experiments. *Appl. Phys. Lett.* **2005**, *87*, 033109.
(10) Ambrosio, A.; Camposeo, A.; Maddalena, P.; Patanè, S.; Allegrini, M. Real- Time Monitoring of the Surface Relief Formation on Azo-Polymer Films Upon Near- Field Excitation. *J. Microsc.* **2008**, *229*, 307−312.
(11) Ambrosio, A.; Cefalì, E.; Spadaro, S.; Patanè, S.; Allegrini, M.; Albert, D.; Oesterschulze, E. Noncontact Tuning Fork Position Sensing for Hollow-Pyramid Near-Field Cantilevered Probes. *Appl. Phys. Lett.* **2006**, *89*, 163108.
(12) Ocelic, N.; Huber, A.; Hillenbrand, R. Pseudoheterodyne Detection for Background-Free Near-Field Spectroscopy. *Appl. Phys. Lett.* **2006**, *89*, 101124.
(13) Gerber, J. A.; Berweger, S.; O'Callahan, B. T.; Raschke, M. B. Phase-Resolved Surface Plasmon Interferometry of Graphene. *Phys. Rev. Lett.* **2014**, *113*, 055502.
(14) Garcia, R.; Herruzo, E. T. The Emergence of Multifrequency Force Microscopy. *Nat. Nanotechnol.* **2012**, *7*, 217−226.
(15) Damircheli, M.; Payam, A. F.; Garcia, R. Optimization of Phase Contrast in Bimodal Amplitude Modulation AFM. *Beilstein J. Nanotechnol.* **2015**, *6*, 1072−1081.
(16) Lozano, J. R.; Garcia, R. Theory of Multifrequency Atomic Force Microscopy. *Phys. Rev. Lett.* **2008**, *100*, 076102.
(17) Dazzi, A.; Prazeres, R.; Glotin, F.; Ortega, J. M. Local Infrared Microspectroscopy with Subwavelength Spatial Resolution with an Atomic Force Microscope Tip Used as a Photothermal Sensor. *Opt. Lett.* **2005**, *30*, 2388−2390.
(18) Lu, F.; Jin, M.; Belkin, M. A. Tip-Enhanced Infrared Nanospectroscopy via Molecular Expansion Force Detection. *Nat. Photonics* **2014**, *8*, 307−312.
(19) Yang, H. U.; Rashcke, M. B. Resonant Optical Gradient Force Interaction for Nano-Imaging and -Spectroscopy. *New J. Phys.* **2016**, *18*, 053042.
(20) Xu, X. G.; Ghamsari, B. G.; Jiang, J.-H.; Gilburd, L.; Andreev, G. O.; Zhi, C.; Bando, y.; Golberg, D.; Berini, P.; Walker, G. C. One-Dimensional Surface Phonon Polaritons in Boron Nitride Nanotubes. *Nat. Commun.* **2014**, *5*, 4782.
(21) Li, P.; Lewin, M.; Kretinin, A. V.; Caldwell, J. D.; Novoselov, K. S.; Taniguchi, T.; Watanabe, K.; Gaussmann, F.; Taubner, T. Hyperbolic Phonon-Polaritons in Boron Nitride for Near-Field Optical Imaging and Focusing. *Nat. Commun.* **2015**, *6*, 7507.
(22) Low, T.; Chaves, A.; Caldwell, J. D.; Kumar, A.; Fang, N. X.; Avouris, P.; Heinz, T. F.; Guinea, F.; Martin-Moreno, L.; Koppens, F. Polaritons in Layered Two- Dimensional Materials. *Nat. Mater.* **2017**, *16*, 182−194.
(23) Yoxall, E.; Schnell, M.; Nikitin, A. Y.; Txoperena, O.; Woessner, A.; Lundeberg, M. B.; Casanove, F.; Hueso, L. E.; Koppens, F. H. L.; Hillebrand, R. Direct Observation of Ultraslow Hyperbolic Polariton Propagation with Negative Phase Velocity. *Nat. Photonics* **2015**, *9*, 674−678.
(24) Basov, D. N.; Fogler, M. M.; Garcia de Abajo, F. J. Polaritons in van der Waals Materials. *Science* **2016**, *354*, 195.
(25) Shi, Z.; Bechtel, H. A.; Berweger, S.; Sun, Y.; Zeng, B.; Jin, C.; Chang, H.; Martin, M. C.; Raschke, M. B.; Wang, F. Amplitude-and Phase-Resolved Nanospectral Imaging of Phonon Polaritons in Hexagonal Boron Nitride. *ACS Photonics* **2015**, *2*, 790−796.
(26) Dai, S.; Ma, Q.; Liu, M. K.; Andersen, T.; Fei, Z.; Goldflam, M. D.; Wagner, M.; Watanabe, K.; Taniguchi, T.; Thiemens, M.; Keilmann, F.; Janssen, G. C. A. M.; Zhu, S.-E.; Jarillo-Herrero, P.; Fogler, M. M.; Basov, D. N. Graphene on Hexagonal Boron Nitride as a Tunable Hyperbolic Metamaterial. *Nat. Nanotechnol.* **2015**, *10*, 682−686.
(27) Kumar, A.; Low, T.; Fung, K. H.; Avouris, P.; Fang, N. X. Tunable Light−Matter Interaction and the Role of Hyperbolicity in Graphene−hBN system. *Nano Lett.* **2015**, *15*, 3172−3180.
(28) Caldwell, J. D.; Kretinin, A. V.; Chen, Y.; Giannini, V.; Fogler, M. M.; Francescato, Y.; Ellis, C. T.; Tischler, J. G.; Woods, C. R.; Giles, A. J.; Hong, M.; Watanabe, K.; Taniguchi, T.; Maier, S. A.; Kostya, S. Hyperbolic Phonon-Polaritons in Boron Nitride for Near-Field Optical Imaging and Focusing. *Nat. Commun.* **2015**, *5*, 5221.
(29) Giles, A. J.; Dai, S.; Glembocki, O. J.; Kretinin, A. V.; Sun, Z.; Ellis, C. T.; Tischler, J. G.; Taniguchi, T.; Watanabe, K.; Fogler, M. M.; Novoselov, K. S.; Basov, D. N.; Caldwell, J. D. Imaging of Anomalous Internal Reflections of Hyperbolic Phonon-Polaritons in Hexagonal Boron Nitride. *Nano Lett.* **2016**, *16*, 3858−3865.
(30) Dai, S.; Ma, Q.; Andersen, T.; Mcleod, A. S.; Fei, Z.; Liu, M. K.; Wagner, M.; Watanabe, K.; Taniguchi, T.; Thiemens, M.; Keilmann, F.; Jarillo-Herrero, P.; Fogler, M. M.; Basov, D. N. Subdiffractional Focusing and Guiding of Polaritonic Rays in a Natural Hyperbolic Material. *Nat. Commun.* **2015**, *6*, 6963.
(31) Dai, S.; Fei, Z.; Ma, Q.; Rodin, A. S.; Wagner, M.; McLeod, A. S.; Liu, M. K.; Gannett, W.; Regan, W.; Watanabe, K.; Taniguchi, T.; Thiemens, M.; Dominguez, G.; Castro Neto, A. H.; Zettl, A.; Keilmann, F.; Jarillo-Herrero, P.; Fogler, M. M.; Basov, D. N. Tunable Phonon Polaritons in Atomically Thin van der Waals Crystals of Boron Nitride. *Science* **2014**, *343*, 1125−1129.
(32) Li, P.; Yang, X.; Maß, T. W. W.; Hanss, J.; Lewin, M.; Michel, A.-K. U.; Wuttig, M.; Taubner, T. Reversible Optical Switching of Highly Confined Phonon-Polaritons with an Ultrathin Phase-Change Material. *Nat. Mater.* **2016**, *15*, 870−876.
(33) Atkin, J. M.; Berweger, S.; Jones, A. C.; Raschke, M. B. Nano-Optical Imaging and Spectroscopy of Order, Phases, and Domains in Complex Solids. *Adv. Phys.* **2012**, *61*, 745−842.
(34) Govyadinov, A. A.; Mastel, S.; Golmar, F.; Chuvilin, A.; Carney, S. P.; Hillenbrand, R. Recovery of Permittivity and Depth from Near-Field Data as a Step Toward Infrared Nanotomography. *ACS Nano* **2014**, *7*, 6911−6921.
(35) Amenabar, I.; Poly, S.; Goikoetxea, M.; Nuansing, W.; Lasch, P.; Hillenbrand, R. Hyperspectral Infrared Nanoimaging of Organic Samples Based on Fourier Transform Infrared Nanospectroscopy. *Nat. Commun.* **2017**, *8*, 14402.
(36) Gilburd, L.; Kim, K. S.; Ho, K.; Trajanoski, D.; Maiti, A.; Halverson, D.; de Beer, S.; Walker, G. C. Hexagonal Boron Nitride Self-Launches Hyperbolic Phonon Polaritons. *J. Phys. Chem. Lett.* **2017**, *8*, 2158−62.
(37) Xu, X. G.; Gilburd, L.; Walker, G. C. Phase stabilized homodyne of infrared scattering type scanning near-field optical microscopy. *Appl. Phys. Lett.* **2014**, *105*, 263104.
(38) Xu, X. G.; Gilburd, L.; Bando, Y.; Golberg, D.; Walker, G. C. Defects and Deformation of Boron Nitride Nanotubes Studied by Joint Nanoscale Mechanical and Infrared Near-Field Microscopy. *J. Phys. Chem. C* **2016**, *120*, 1945−51.
(39) Gilburd, L.; Xu, X. G.; Bando, Y.; Golberg, D.; Walker, G. C. Near-field infrared pump−probe imaging of surface phonon coupling in boron nitride nanotubes. *J. Phys. Chem. Lett.* **2016**, *7*, 289−94.
(40) Wang, L.; Wang, H.; Wagner, M.; Yan, Y.; Jakob, D. S.; Xu, X. G. Nanoscale simultaneous chemical and mechanical imaging via peak force infrared microscopy. *Sci. Adv.* **2017**, *3*, e1700255.
(41) Shen, S.; Narayanaswamy, A.; Chen, G. Surface Phonon Polaritons Mediated Energy Transfer between Nanoscale Gaps. *Nano Lett.* **2009**, *9*, 2909−2913.

DOI: 10.1021/acsnano.7b02323
ACS Nano 2017, 11, 8741−8746

(42) Rousseau, E.; Siria, A.; Jourdan, G.; Volz, S.; Comin, F.; Chevrier, J.; Greffet, J. J. Surface Phonon Polaritons Mediated Energy Transfer between Nanoscale Gaps. *Nat. Photonics* **2009**, *3*, 514−517.
(43) Nowak, D.; Morrison, W.; Kumar Wickramasinghe, H.; Jahng, J.; Potma, E.; Wan, L.; Ruiz, R.; Albrecht, T. R.; Schmidt, K.; Frommer, J.; Sanders, D. P.; Park, S. Nanoscale Chemical Imaging by Photoinduced Force Microscopy. *Sci. Adv.* **2016**, *2*, e1501571.
(44) Dazzi, A.; Prater, C. B. AFM-IR: Technology and Applications in Nanoscale Infrared Spectroscopy and Chemical Imaging. *Chem. Rev.* **2017**, *117*, 5146−5173.
(45) Wang, L.; Meric, I.; Huang, P. Y.; Gao, Q.; Gao, Y.; Tran, H.; Taniguchi, T.; Watanabe, K.; Campos, L. M.; Muller, D. A.; Guo, J.; Kim, P.; Hone, J.; Shepard, K. L.; Dean, C. R. One-dimensional Electrical Contact to a Two-Dimensional Material. *Science* **2013**, *342*, 614−617.

DOI: 10.1021/acsnano.7b02323
ACS Nano 2017, 11, 8741−8746

Mechanical Detection and Imaging of Hyperbolic Phonon Polaritons in Hexagonal Boron Nitride: Supporting Information

Antonio Ambrosio,[1,2,3] Luis A. Jauregui,[2] Siyuan Dai,[4] Kundan Chaudhary,[5] Michele Tamagnone,[5] Michael Fogler,[4] Dimitri N. Basov,[4,6] Federico Capasso,[5] Philip Kim[2] and William L. Wilson[1]

[1]*Center for Nanoscale Systems, Harvard University, Cambridge, Massachusetts 02138, USA*

[2]*Department of Physics, Harvard University, Cambridge, Massachusetts 02138, USA*

[3]*CNR-SPIN U.O.S. Napoli, Complesso Universitario di Monte Sant'Angelo, Via Cintia, 80126 – Napoli, Italy*

[4]*Department of Physics University of California, San Diego (UCSD)*

[5]*Harvard John A. Paulson School of Engineering and Applied Sciences, Harvard University, Cambridge, Massachusetts 02138, USA*

[6]*Department of Physics, Columbia University, 538 West 120th Street, New York, New York 10027, United States*

corresponding author: ambrosio@seas.harvard.edu

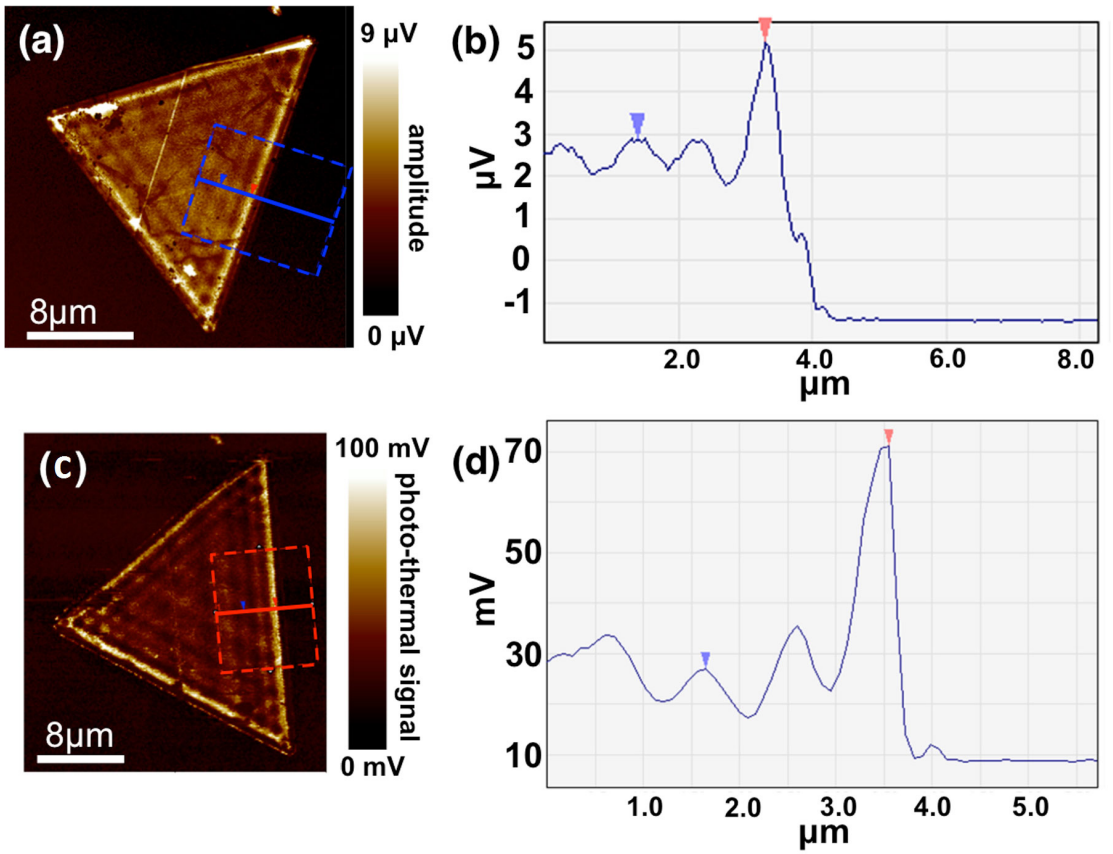

Figure S1 – (a) Scattering near-field optical image of a triangle-shaped hBN flake (Amplitude). The flake is the same of Figure 1 of the main text. (b) Profile along the blue line of Figure S1 (a) (averaged in the dashed blue contour area). (c) and (d) same as (a) and (b) for the photo-thermal image obtained by monitoring the microscope probe oscillations around 170kHz. The periodicity of the phonon polariton interference pattern (half of the distance between the blue and red arrows in the images) is 850nm for both (b) and (d). Moreover, the fringes position with respect to the flake edge are the same in both (b) and (d), within an error of 50nm.

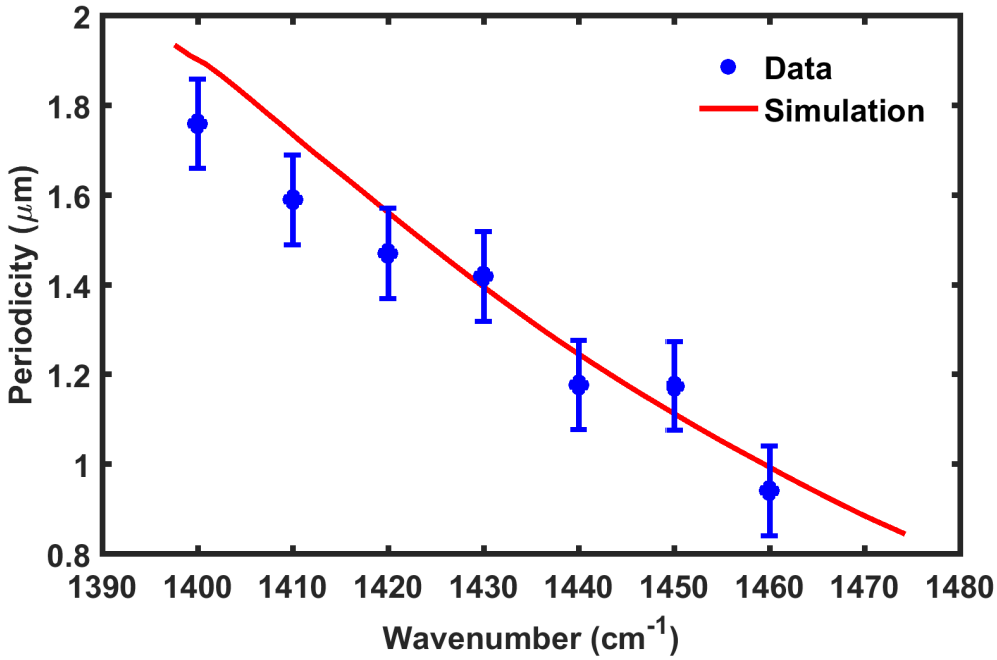

Figure S2 – Periodicity of the phonon polariton interference pattern as a function of the illuminating light wavenumber for the disk-shaped hBN flake of Figure 2. The flake is on a Si substrate without any SiO_2 layer. The simulations were done using Lumerical FDTD, modelling h-BN with an anisotropic Lorentz model [27]. The error bars are 0.2μm.

Artifacts in case of high laser power conditions

When the illuminating laser power is high (about 1mW), the topography image may also show the same features of the photo-thermal image, with the topography peaks corresponding to the peaks of the induced mechanical oscillations (Figure S3). Also, the surface of the sample is usually damaged after scanning in such conditions, with permanent deformations (Figure S3). Looking at the topographical deformation during photo-thermal imaging, the variation is close to 20% of the sample thickness with an apparent reduction of the sample height (see also Figure S4). Although the sign of the thermal deformation may be compatible with the negative thermal constant components of hBN,[1] such morphology variation, if true, would need a temperature variation so high to actually melt the sample. We believe, in fact, that the significant morphology deformation measured is an artifact due to our high-power operating conditions and the presence of water. In fact, the same sample after thermal annealing produces less or not at all modulation of the sample topography (Figure S5). To understand the possible artifact mechanism, it is important to consider that AFM is operated in contact mode (the contact is continuous during scanning). It is quite different from tapping mode used in scattering SNOM where the tip oscillates at about 300kHz with intermittent contact with the surface and an average distance of tens of nanometers. We believe that the local heating associated to the phonon polariton maxima may affects, besides the crystal lattice, also the water layer on the surface (water meniscus) and the intra-layer water in the flake. This can result in a local change of the interaction between the sample surface and the microscope probe that is in fact interpreted by the microscope feedback system as a local change of the sample height. Moreover, the sample height after the photo-thermal imaging in these

experimental conditions (high laser power) is found to be a few nanometers higher than the original (Figure S4) while the lateral dimensions of the flake never change. These results clearly support the thermal origin of our imaging mechanism.

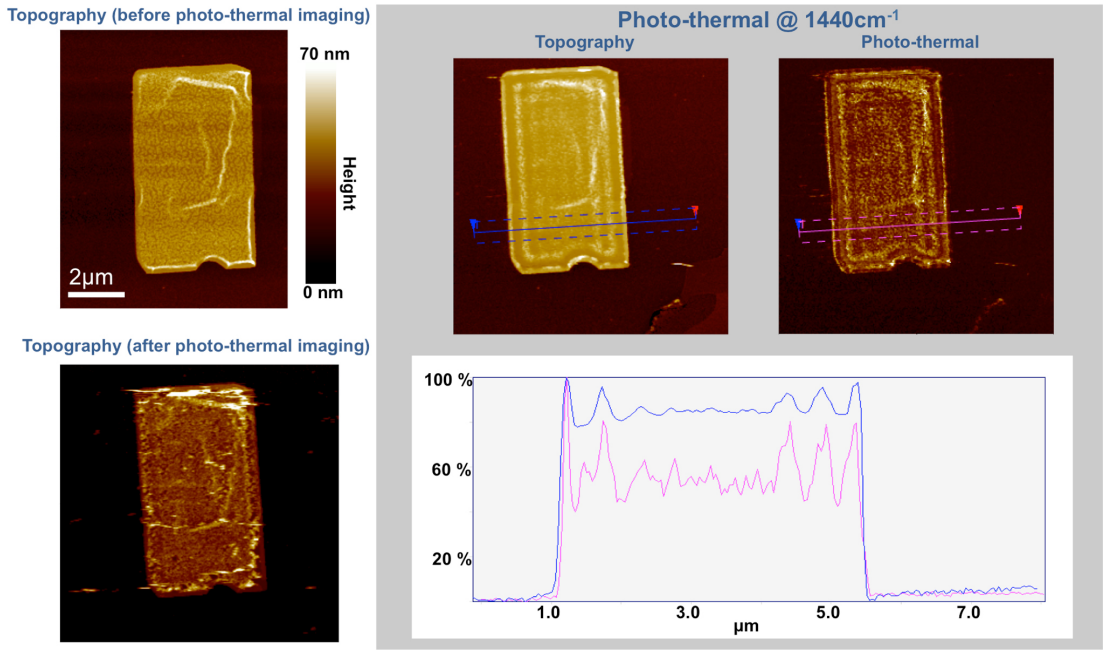

Figure S3 – (a) Topography image of a rectangle-shaped hBN flake of dimensions 4.4μm×7.6μm on 285nm thick SiO_2. The flake in (a) was never exposed to laser light before. (b) and (c) topography and photo-thermal image recorded during the photo-thermal imaging with a laser power up to 20% of the maximum (about 1mW). It is evident that the same features are present in both topography and photo-thermal images. This is also highlighted in the plot (d) where a cross section of the topography image is compared with the profile of the photo-thermal image. The ordinate values are reported in percent of the higher value since the purpose of this plot is only to compare the features' positions. From this, it is evident that the peaks in topography correspond to the peaks in the photo-thermal image. (e) Topography of the flake after photo-thermal imaging (no laser is sent to the microscope). The surface of the flake is now rougher compared to the pristine condition of (a) with some topographical

features that still resemble the features in (b) and (c). This is an evidence of the thermal nature of the process and the permanent alteration of the sample surface in these “high-laser-power” experimental conditions. The time between the first image with light off (“Topography before photo-thermal imaging”) and the second image with light off (“Topography after photo-thermal imaging”) is the time needed to take the photo-thermal image at 1440cm^{-1} that is 50 minutes.

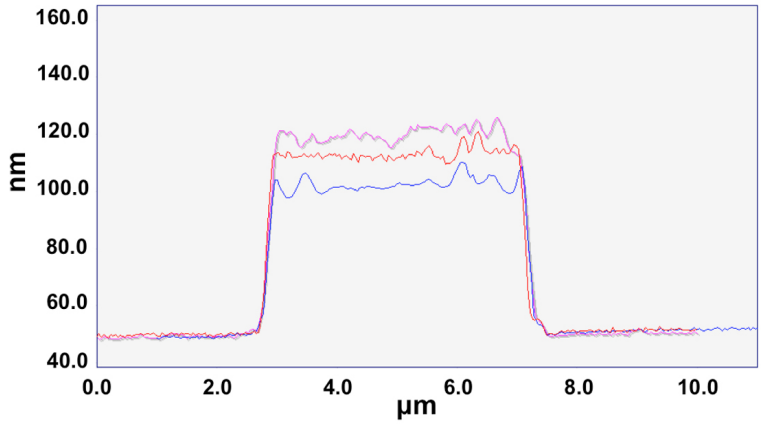

Figure S4 – Topography profiles of the flake in Figure S3. (Red) pristine conditions, sample never exposed to light. (Blue) Topography recorded during photo-thermal imaging. (Pink) Topography recorded after photo-thermal imaging.

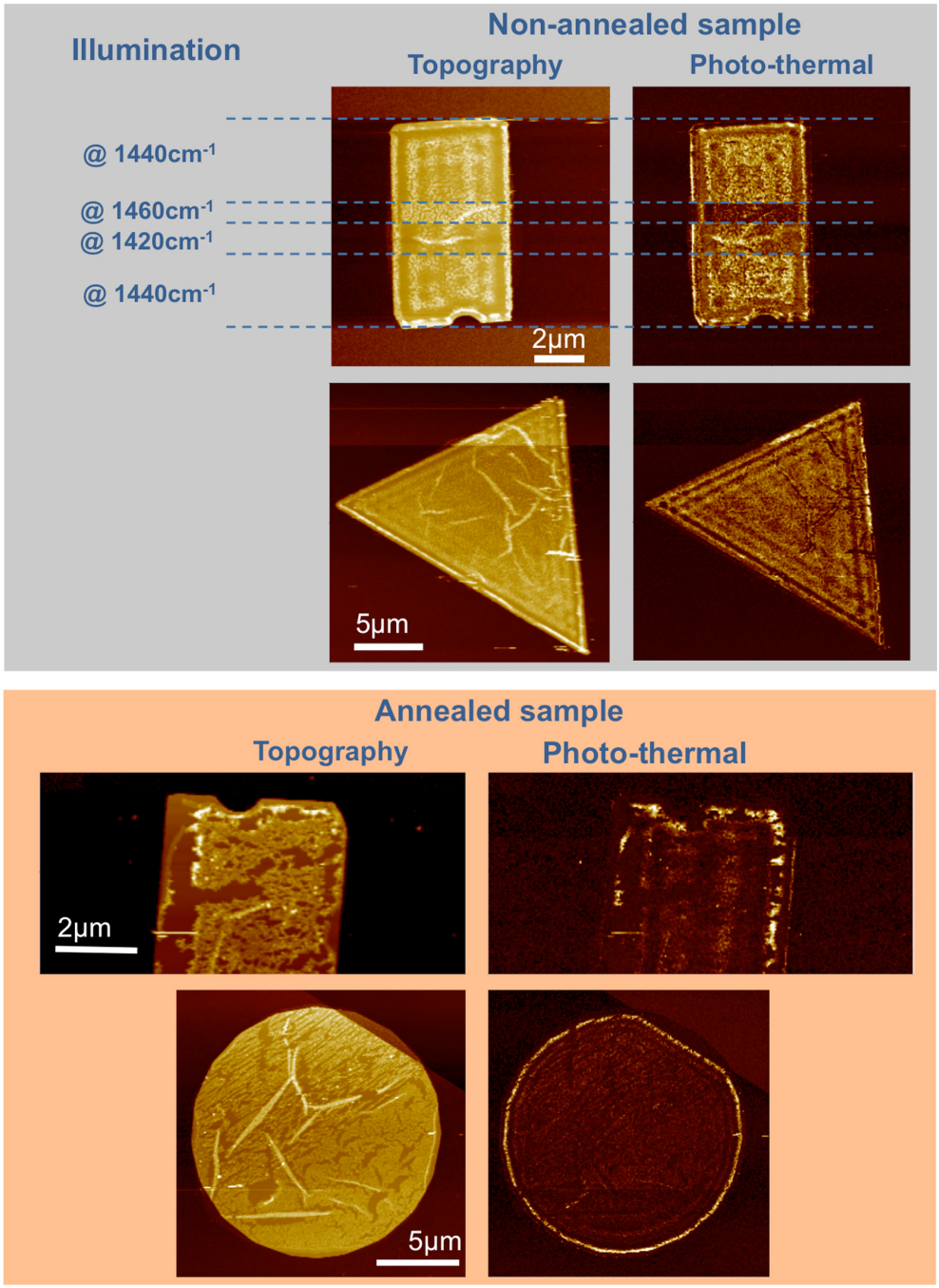

Figure S5 – Topography and photo-thermal signal for several shaped-flakes before and after the thermal annealing. The Topography deformation resembling the phonon polariton pattern is only visible for before-annealing samples. The residuals visible in topography are from the lithography process and are created during the h-BN dry etching process, which is performed using a fluorine based chemistry (see full process description in the main text). During this process, the resist is also slightly etched, and, being organic, it produces a PTFE-like fluorinated residue which is resistant to

the Remover PG and chloroform and therefore remains on the sample. For the image at different illuminating light wavenumbers, the wavelength of the incident light was changed while scanning.

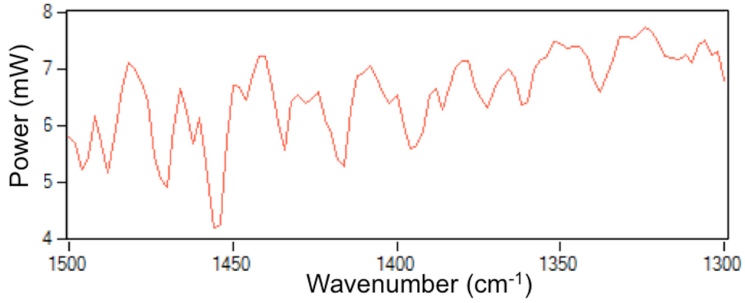

Figure S6 – Laser Power as a function of the wavelength (wavenumbers in cm^{-1}). This power is measured inside the microscope far from the sample. In this commercial setup the power illuminating the sample cannot be tuned continuously. The user can only choose between definite percentage values of power illuminating the sample that represents only an upper limit of the power that is in fact illuminating the sample. The laser is focused on the sample by means of a low NA parabolic mirror at 70° from the vertical to the sample surface.

Nano-imaging and spectra collection

In both the s-SNOM setup and the photo-thermal setup used, nano-imaging is obtained by selecting a single wavelength for the illuminating light and scanning the sample under the microscope probe that is aligned to the illuminating light. Instead, the approaches to obtain a spectrum in a specific position in the scanning area are different in s-SNOM and photo-thermal.

In s-SNOM the CW QCL source is changed with a pulsed DFG laser and a longer interferometer is used to produce an interferogram that is then turned into a spectrum by means of Fourier Transform.

For the photo-thermal setup instead, a spectrum can be obtained by swiping the illuminating light wavelength across the laser emission wavelengths range.

In both setups it is not possible to produce a hyperspectral image with the same resolution of an image at a single wavelength. In fact, the positioning of the probe on a specific location of the sample is done by first producing a topographical map of the sample, used then as map to navigate the surface, while the image of the polariton fringes is not available for tip positioning.

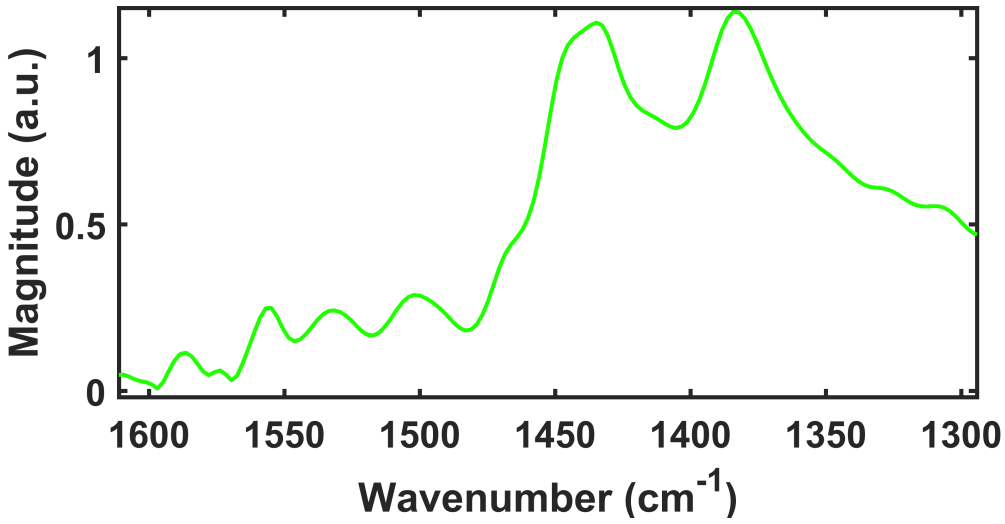

Figure S7 – Amplitude of the s-SNOM signal as a function of the illuminating light wavelength (nano-FTIR) when the tip of the microscope probe is on a position close to the edge of an hBN on SiO_2. The number of peaks and the strength of each peak depends upon the specific position on the flake and the distance from the edge.

(1) Belenkii, G.L.; Salaev, E. Y. The Nature of Negative Linear Expansion in Layer Crystals C, Bn, GaS, GaSe and InSe. Suleimanov, R.A.; Abdullaev, N.A.; Shteinshraiber, V.Y. *Solid State Communications* **1985**, *53*, 967-971.